論文 / 著書情報
Article / Book Information

Title	3-D electromagnetic imaging of highly deformed fluid-rich weak zones and locked section of the North Anatolian fault beneath the Marmara Sea
Authors	Kaya-Eken Tulay, Yasuo Ogawa, Yoshiya Usui, Takafumi Kasaya, M. Kemal Tunçer, Yoshimori Honkura, Naoto Oshiman, Masaki Matsushima, Weerachai Siripunvaraporn
Citation	Geology, Volume 54, Number 3, pp. 200-204
Pub. date	2026, 3
DOI	https://dx.doi.org/10.1130/G52995.1
Creative Commons	See next page.

License

GEOLOGY | THE GEOLOGICAL SOCIETY OF AMERICA®

https://doi.org/10.1130/G52995.1

Manuscript received 12 June 2025
Revised manuscript received 8 October 2025
Manuscript accepted 21 November 2025

Published online 8 December 2025

3-D electromagnetic imaging of highly deformed fluid-rich weak zones and locked section of the North Anatolian fault beneath the Marmara Sea

Tülay Kaya-Eken[1,2,3,*], Yasuo Ogawa[2,4,*], Yoshiya Usui[5], Takafumi Kasaya[6], M. Kemal Tunçer[7], Yoshimori Honkura[1,2], Naoto Oshiman[8], Masaki Matsushima[9], and Weerachai Siripunvaraporn[10]

[1]Earth and Planetary Sciences, Tokyo Institute of Technology, Tokyo 152-8551, Japan
[2]Volcanic Fluid Research Center, Tokyo Institute of Technology, Tokyo 152-8551, Japan
[3]Department of Geodesy, Boğaziçi University, İstanbul 34684, Türkiye
[4]Research Center for Prediction of Earthquakes and Volcanic Eruptions, Graduate School of Science, Tohoku University, Sendai 980-8577, Japan
[5]Earthquake Research Institute, The University of Tokyo, Tokyo 113-0032, Japan
[6]IFREE, Japan Agency for Marine-Earth Science and Technology, Yokosuka 237-0061, Japan
[7]Department of Geophysical Engineering, İstanbul University–Cerrahpaşa, İstanbul 34320, Türkiye
[8]Disaster Prevention Research Institute, Kyoto University, Kyoto 611-0011, Japan
[9]Department of Earth and Planetary Sciences, Institute of Science Tokyo, Tokyo 152-8551, Japan
[10]Department of Physics, Faculty of Science, Mahidol University, Bangkok 10400, Thailand

ABSTRACT

Reliable knowledge of the crustal properties beneath the North Anatolian fault (NAF), seismically silent for more than 250 years beneath the Marmara Sea (MS), is crucial for understanding seismic hazard and mitigating the potential for disaster on an enormous scale. In the present work, the first three-dimensional inverse modeling performed on a magnetotelluric dataset of the MS has unveiled localized weak and locked fault segments along this shear deformation zone. Low-resistivity regions along the northern branch of the NAF beneath the Central and Çınarcık-Imralı basins are likely attributed to the presence of fluids, which may represent a fault zone conductor in a fractured zone and can explain the densely populated microseismicity. These low-resistivity anomalies surrounded by higher resistivity structures imply that the segmented, multi-branched NAF system extends beneath the MS, following the Intra-Pontide suture zone. The resistive anomalies, between the Central and Çınarcık basins, along with those at the western and eastern extremities of the MS, presumably signify regions of stress accumulation, shedding light on the ongoing processes of fault mechanics at play in this critical region.

INTRODUCTION

The tectonic configuration of Türkiye (Fig. 1) is the consequence of the complex interplay of various tectonic events, including rifting, collision, and subduction, developed due to the evolution of the Tethys system. The closure of Paleo-Tethys led to the formation of the Intra-Pontide suture zone, the Marmara Sea (MS), and adjacent tectonic blocks: the Istanbul–Zonguldak Zone, Armutlu–Almacık Zone, and Sakarya Continent.

The MS region occupies a unique tectonic position, straddling the extensional regime of western Anatolia and the shearing forces of the North Anatolian fault (NAF) system, extending over ~1500 km through northern Türkiye, following the trace of the older Intra-Pontide suture zone (Şengör et al., 2005). While branches of the NAF passing through the three tectonic zones on land (Fig. 1) are well documented (Yılmaz et al., 1997), the extent of these zones and the NAF system into the MS remains poorly understood (Bécel et al., 2009).

Previous investigations on historical earthquakes (Barka, 1999) highlight a pattern of westward-moving destructive earthquakes along the NAF since 1939 (Fig. S1 in the Supplemental Material[1]), with the two recent ruptures in this sequence occurring in 1999 near the eastern edge of the MS (Fig. 1). Given this pattern and accumulated stress transferred from the 1999 İzmit earthquake, the MS is likely to be the location of the next large rupture on the NAF (Hubert-Ferrari et al., 2000). The 2019 (Mw 5.7) and 2025 (Mw 6.2) failures within the Kumburgaz basin of the MS are notable to show the stress accumulation potential of this region (Irmak et al., 2021). Recent studies (Schmittbuhl et al., 2016) have provided insight into the depth profile of the NAF within the crust. However, there is still limited knowledge about the structural characteristics of the crust, mainly stemming from the inadequate seismic coverage in this area due to the absence of offshore seismic stations.

Tülay Kaya-Eken https://orcid.org/0000-0002-6439-6759
Yasuo Ogawa https://orcid.org/0000-0002-6663-401X
*Corresponding authors: tulay.kaya@bogazici.edu.tr; yasuo.ogawa.d1@tohoku.ac.jp

[1]Supplemental Material. 3-D electromagnetic imaging of highly deformed fluid-rich weak zones and locked section of the North Anatolian Fault beneath the Marmara Sea (the data and modeling in detail). Please visit https://doi.org/10.1130/GEOL.S.30715481 to access the supplemental material; contact editing@geosociety.org with any questions.

CITATION: Kaya-Eken, T., et al., 2026, 3-D electromagnetic imaging of highly deformed fluid-rich weak zones and locked section of the North Anatolian fault beneath the Marmara Sea: Geology, v. 54, p. 200–204, https://doi.org/10.1130/G52995.1

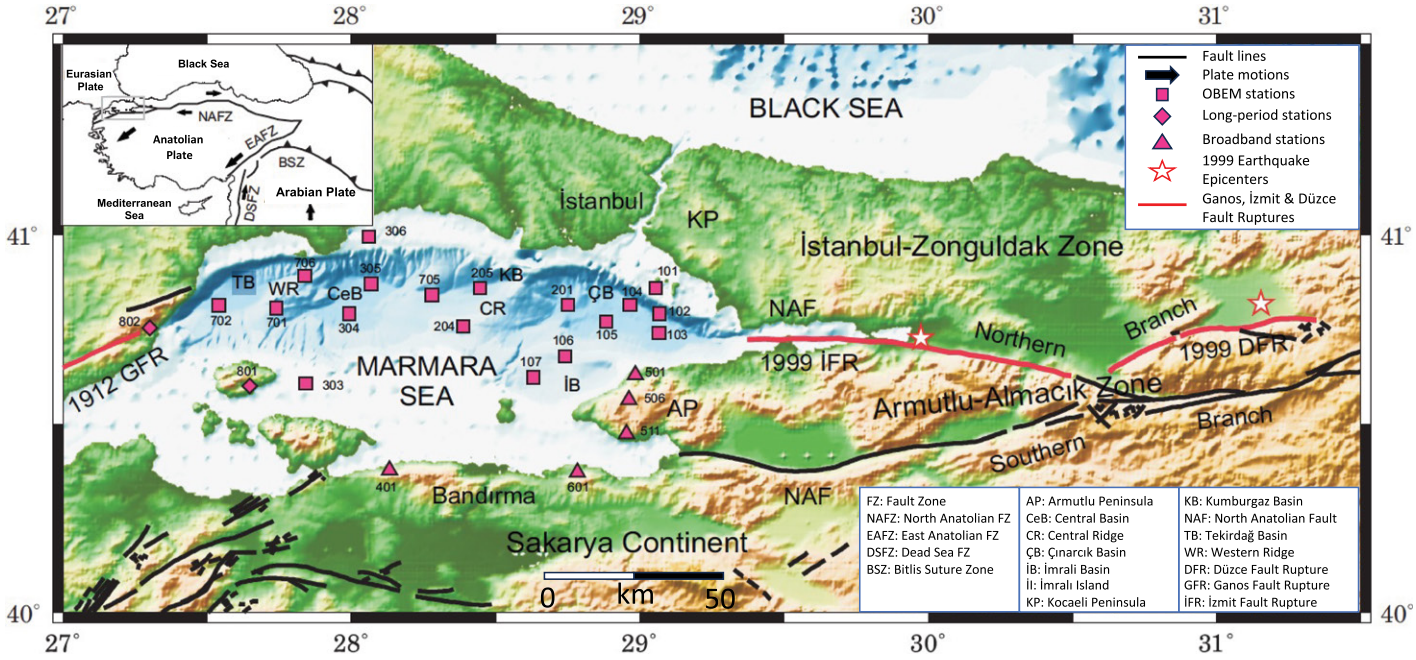

Figure 1. Location map of magnetotelluric sites within and around the Marmara Sea. Inset: Tectonic map of Türkiye with the study area outlined by the gray rectangle. OBEM—ocean-bottom electromagnetic.

To improve our understanding of the tectonic forces causing the earthquakes, knowledge on the rheological structure of the lithosphere is required. Magnetotelluric (MT) modeling provides an efficient tool for detecting the presence of fluids affecting subsurface rheology and resolving the geometries and electrical properties of lithospheric structures (Wannamaker et al., 2009). Previous MT studies performed around active fault zones have demonstrated a strong correlation between seismic activity and the presence of fluids, as inferred from variations in electrical resistivity (Unsworth et al., 1997; Ogawa and Honkura, 2004; Karcıoğlu et al., 2013). The first electromagnetic study in the MS, earlier conducted by Kaya et al. (2013), provided two-dimensional (2-D) geoelectrical images around the Çınarcık basin and revealed the fluid distribution 10 km below the NAF. Fluids are interpreted to exist at depths shallower than 20 km within the crust, while low-resistivity anomalies in the deeper crust may be related to saline fluid and partial melting.

In the present work, we performed three-dimensional (3-D) MT modeling using a combined dataset in and around the MS to elucidate a high-resolution resistivity distribution that will facilitate a deeper understanding of the geodynamic system, the lithospheric structures and the westward extension of the NAF system into the MS, and tectonic structures that could accumulate stress for the next possible rupture.

MT DATA AND MODELING

Ocean-bottom electromagnetic, broadband, and long-period MT data collected at 25 sites in and around the MS (Figs. 1 and S2), including the data utilized in an early 2-D MT modeling study of Kaya et al. (2013), were jointly inverted using a 3-D inversion code with an unstructured tetrahedral mesh (Usui, 2015; Usui et al., 2018) for the periods $10 < T < 8200$ s to investigate crustal and upper mantle structures. The details on the data and modeling are provided in the Supplemental Material.

RESULTS, INTERPRETATION, AND DISCUSSION

Geological Character of the Observed Anomalies and the Effect of Fluid

Figure 2 displays the final 3-D electrical resistivity model using representative horizontal depth slices and vertical cross sections for the seismogenic upper crust, lower crust, and upper mantle beneath the MS. The conductive structures (<10 Ωm) at shallow depths up to 6 km (Figs. 2C and 3) represent Ordovician to Carboniferous sedimentary rocks (Yılmaz et al., 1997). The resistive anomalies R1 (>1000 Ωm) and R3 (>300 Ωm) indicate the locations of the Central and Western ridges in the MS (Fig. 2C). The resistor, R2, to the northeast of the Çınarcık basin, corresponds to part of the Istanbul–Zonguldak Zone consisting of Precambrian bedrock deposits with a lack of significant deformation (Görür et al., 1997), while the southern resistor, R4, corresponds to the variably metamorphosed bedrock deposits of the Sakarya Continent (Fig. 2A). The resistive and conductive zones beneath the Armutlu Peninsula (Fig. 2A) represent high- and low-grade metamorphic succession (Yılmaz et al., 1997) at shallow (<20 km) and interconnected fluid at deeper depths (>20 km).

The high conductive anomalies (<10 Ωm) along the probable branches of the NAF (<5 km) are consistent with relatively low S-wave velocity (Turunçtur et al., 2023) and probably represent a highly deformed and fluid-rich zone (C1) of the NAF (Fig. 2). This fluid could be associated with the penetration of seawater into the deformed zone or a deeper source (Fig. 3). The low-resistivity anomalies C2 and C3 display vertical structures extending from ~5 km to the upper mantle depths (Fig. 2C). The estimated porosity of ~10% for C2 and C3 (see Supplemental Material) may suggest the presence of aqueous fluids, which have been shown to weaken the brittle crust (Wannamaker et al., 2009). Precise hypocenter locations of the microseismic activity beneath the MS (Wollin et al., 2018) correspond with these conductive anomalies down to a depth of ~20 km (Fig. 2), implying that C2 and C3 are related to interconnected fluid pathways. The high Vp/Vs ratio and low Vs values for the top 10–15 km beneath the Çınarcık-İmralı basin and Central basin and low-velocity zones at shallow depths were observed in recent tomography studies (Barış et al., 2005; Tarancıoğlu et al., 2020). They confirm our high-conductivity anomalies, some imaged earlier along the 2-D MT profile by Kaya et al. (2013) and attributed to upwelling fluids through the crust. Similar to resistivity variation beneath the MS, Becken et al. (2011) found a sub-vertical conductive zone beneath the San Andreas fault, interpreted as a source of fluid in the upper crust, and a resistive block representing the locked seg-

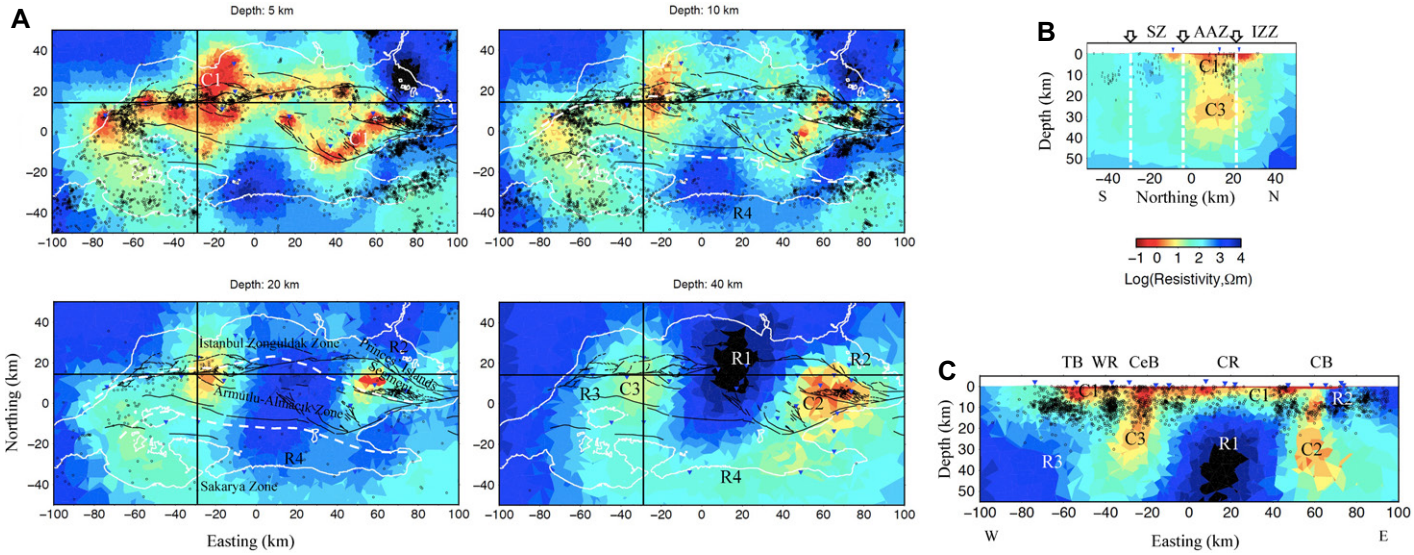

Figure 2. Final 3-D electrical resistivity model. (A) Plan view sections for representative depths. Blue triangles represent the location of stations. Black and white dashed lines show the fault branches in the Marmara Sea and the surface limit of the Intra-Pontide suture zone (modified from Le Pichon et al., 2014). (B) N–S cross section along −30 km E profile shown by the black line on the plan view. White dashed lines with white arrows show possible branches of the North Anatolian fault. (C) E–W cross section along 15 km N profile shown by the black line on the plan view. C and R represent conductors and resistors, respectively. Black dots show seismic events with M <5 recorded between 2000 and 2016 (Kandilli Observatory and Earthquake Research Institute, http://www.koeri.boun.edu.tr/sismo/zeqdb/). AAZ—Armutlu–Almacık Zone; IZZ—Istanbul-Zonguldak Zone; SZ—Sakarya Zone; CeB—Central basin; ÇB—Çınarcık basin; CR—Central Ridge; TB—Tekirdağ basin; WR—Western Ridge.

ment of the San Andreas fault. Hence, we suggest that the observed pattern of seismicity and seismic velocity anomalies integrated with the resistivity distribution (Fig. 2) in this work likely indicate fluid intrusion into the fault zone activity and fluid over-pressure due to the existence of less permeable crust, which can reduce the effective normal stress and thus the shear stress required to trigger frictional instability (Özaydın et al., 2018). The resultant over-pressurization in the brittle seismogenic parts of the fault causes an increasing activity for microearthquakes (Schiffer et al., 2019).

In the resistivity model spanning depths of 5–40 km (Fig. 2A), the conductive anomalies are situated between the potential branches of the NAF within the MS region. Their alignment closely mirrors the trace of the Intra-Pontide suture as described in Le Pichon et al. (2014). This correspondence supports that C2 and C3 anomalies may represent fractured zones of the NAF beneath the MS.

Implications for the Seismogenic Zone Properties

Extensive research has been conducted on the unruptured segment of the Main Marmara fault beneath the MS, covering a distance of ~150 km. These studies mainly examined integrated data involving the spatiotemporal characteristics of microseismic activity in this region and geodetic constraints mainly from the GPS analyses (Bohnhoff et al., 2013; Jolivet et al., 2023). However, the inadequate seismic coverage in this area due to the absence of offshore seismic stations and imaging efforts on earthquake activities with hypocentral depths only down to 0–25 km limit the vertical resolution. In this regard, an MT model provides a complementary tool because it considerably enhances the knowledge of the depth extent of the crustal and lithospheric structure beneath the MS.

The spatial distribution of the earthquake magnitude-frequency relationship implied that the western part is undergoing a transition from a creeping aseismic state to a potentially seismogenic state toward the east along the Main Marmara fault (Schmittbuhl et al., 2016). Activity of the creeping segment and no significant strain accumulation beneath the central section of the Main Marmara fault (a possible branch between the Çınarcık basin and Central basin) commencing from a depth of ~3 km below a locked zone was further reported in Ergintav et al. (2014). This area is characterized by relatively low Vs (Turunçtur et al., 2023) and shallow conductive anomalies in our models. Schmittbuhl et al. (2016) and Lange et al. (2019) identified a locked fault segment beneath the Kumburgaz basin and Çınarcık basin that is compatible with the relatively high resistivities (>300 Ωm) observed between the Central basin and Çınarcık basin (Figs. 2A–2C), where the 2019 (Mw 5.7) and 2025 (Mw 6.2) MS earthquakes took place, and to the north of the Çınarcık basin. Vertical continuation of this highly resistive zone reaches the bottom of the crustal layer, implying the presence of a strong locked zone with a lithospheric extent (Figs. 2B

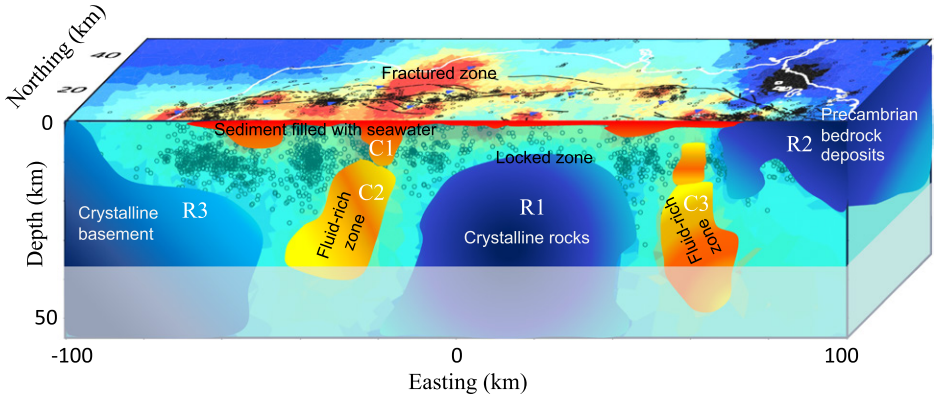

Figure 3. A 3-D view of the magnetotelluric model highlighting its weak (warm-colored), strongly locked (cool-colored), and less sensitive (shaded) areas.

and 2C). Our sensitivity tests, provided in the Supplemental Material (Tables S1–S3 and Figs. S11–S14 and S19–S20), reasonably prove that the data justify these structures.

In general, the final inverted model of this study suggests a westward continuation of the Armutlu–Almacık Zone (Figs. 2B and S4), a weak deformation zone of the NAF system, due to the similar pattern, a sandwiched conductive anomaly between north and south resistors, previously modeled by several MT studies (Tank et al., 2005; Kaya et al., 2009, 2013). Extending the branches of the NAF into the MS following the distribution of seismicity reveals a good correspondence between the branches and boundaries of resistive and conductive zones down to a depth of 20 km (Fig. S4). New constraints of the conductive zones along with high Vp/Vs ratios (Barış et al., 2005) and precisely located seismic clusters (Wollin et al., 2018) focusing around these regions (between 5 km and 15 km) mark presumably weak zones accommodating crustal deformation in the region. These weak zones can be linked to high pore pressures and/or water-filled microcracks (Schiffer et al., 2019), as well as deep creep behavior (5–15 km) in the west of the Main Marmara fault. Our models suggest that, at least to some degree, the boundaries between weak and strong upper crustal domains or the edges of resistive zones can be the nucleation point of a future devastating rupture in the region, since they may focus on deformation. In this respect, the resistive zones between the Çınarcık basin and Central basin and at the eastern and western ends of the MS may be key, as the rupture process of the last two devastating earthquakes, İzmit (Mw 7.4) and Düzce (Mw 7.2), were previously observed to initiate on the resistive side of one of the conductive-resistive boundaries (Tank et al., 2005; Kaya et al., 2009). New high-resolution geoelectrical images of these boundaries and the resistive zones in the area shed a detailed light on the deeper nature of the present seismic gap between the Çınarcık basin and Central basin, which has the potential to produce an earthquake with magnitudes of Mw ~7.2–7.3 between the Çınarcık basin and Central basin, for a fault length of ~60 km, seismogenic depth of 15 km, and slip deficit rates of ~10–15 mm/yr, as inferred from GPS (Ergintav et al., 2014) and 260 years of historical recurrence period (e.g., Parsons, 2004) (see Supplemental Material).

CONCLUSIONS

We present the first 3-D MT model for the MS, providing high-resolution electrical resistivity character beneath the MS down to the depths of crustal and upper mantle structures. Our findings reveal a distinctive geoelectrical feature within the MS: the region of a conductive anomaly surrounded by resistive zones to the north and south that has been previously observed at Düzce, İzmit, and the eastern MS, and that extends westward across the Marmara Region. The significant variation of the electrical properties between resistive and conductive structures vividly highlights the segmented nature of the NAF system extending farther west toward the Central basin. Furthermore, our research identifies the continuation of the three tectonic zones from the western Pontides into the MS, shedding light on the intricate geological dynamics at play. New findings on conductive zones derived from the final inverted model in this study, when considered alongside seismological and geodetic constraints, indicate crustal deformation zones that were weakened through fluid activity (e.g., elevated pore pressures and/or the presence of water-filled microcracks) and/or a deep aseismic creep process of the fault (5–15 km) in the west of the Main Marmara fault. We suggest that future catastrophic ruptures in the area can potentially nucleate at these remarkable conductive-resistive zone boundaries between weaker and stronger upper crustal domains or the edges of these resistive zones. Therefore, the precise imaging of the location and seismic behavior of these resistive zones along fault traces is of great importance for making advanced seismic hazard assessments of a potential large earthquake in the MS.

ACKNOWLEDGMENTS

This study was supported by KAKENHI (grants-in-aid for scientific research; 19253002) and SATREPS (Science and Technology Research Partnership for Sustainable Development)–MarDiM (Earthquake and Tsunami Disaster Mitigation in the Marmara Region and Disaster Education in Türkiye) Project under the Japan International Cooperation Agency and the Japan Science and Technology Agency. We thank the Office of Navigation, Hydrography, and Oceanography of the Turkish Naval Forces, Taisei Corporation, and Turkish Airlines for their assistance during this study, and to the Marine Research Department, MTA (Mineral Research and Exploration), for providing bathymetry data for the MS. In this study, we used the computer systems of the Earthquake and Volcano Information Center of the Earthquake Research Institute, the University of Tokyo. We thank Tuna Eken for his helpful comments, and S. Bülent Tank and Tadanori Goto for their help in data acquisition. We thank Martyn Unsworth, Daniel Diaz, the anonymous reviewer, and editor Tracy Rushmer for their valuable comments and suggestions that improved the manuscript. Some figures were generated using Generic Mapping Tools (Wessel and Smith, 1995).

REFERENCES CITED

Barış, S., Nakajima, J., Hasegawa, A., Honkura, Y., Ito, A., and Ucer, S.B., 2005, Three-dimensional structure of Vp, Vs, and Vp/Vs in the upper crust of the Marmara region, NW Turkey: Earth, Planets, and Space, v. 57, p. 1019–1038, https://doi.org/10.1186/BF03351882.

Barka, A., 1999, The 17 August Izmit earthquake: Science, v. 285, p. 1858–1859, https://doi.org/10.1126/science.285.5435.1858.

Bécel, A., Laigle, M., de Voogd, B., Hirn, A., Taymaz, T., Galve, A., Shimamura, H., Murai, Y., Lepine, J.C., Sapin, M., and Özalaybey, S., 2009, Moho, crustal architecture and deep deformation under the North Marmara Trough, from the SEISMARMARA Leg 1 offshore-onshore reflection-refraction survey: Tectonophysics, v. 467, p. 1–21, https://doi.org/10.1016/j.tecto.2008.10.022.

Becken, M., Ritter, O., Bedrosian, P.A., and Weckmann, U., 2011, Correlation between deep fluids, tremor and creep along the San Andreas fault: Nature, v. 480, p. 87–90, https://doi.org/10.1038/nature10609.

Bohnhoff, M., Bulut, F., Dresen, G., Malin, P.E., Eken, T., and Aktar, M., 2013, An earthquake gap south of Istanbul: Nature Communications, v. 4, 1999, https://doi.org/10.1038/ncomms2999.

Ergintav, S., Reilinger, R.E., Çakmak, R., Floyd, M., Cakir, Z., Doğan, U., King, R.W., McClusky, S., and Özener, H., 2014, Istanbul's earthquake hot spots: Geodetic constraints on strain accumulation along faults in the Marmara seismic gap: Geophysical Research Letters, v. 41, p. 5783–5788, https://doi.org/10.1002/2014GL060985.

Görür, N., Monod, O., Okay, A.I., Şengör, C.A.M., Tüysüz, O., Yiğitbaş, E., Sakınç, M., and Akkök, R., 1997, Palaeogeographic and tectonic position of the carboniferous rocks of the western Pontides (Turkey) in the frame of the Variscan belt: Bulletin de la Société Géologique de France, v. 168, p. 197–206.

Hubert-Ferrari, A., Barka, A., Jacques, E., Nalbant, S.S., Meyer, B., Armijo, R., Tapponnier, P., and King, G.C.P., 2000, Seismic hazard in the Marmara Sea region following the 17 August 1999 İzmit earthquake: Nature, v. 404, p. 269–273, https://doi.org/10.1038/35005054.

Irmak, T.S., Yolsal-Çevikbilen, S., Eken, T., Doğan, B., Erman, C., Yavuz, E., Alcik, H., Gaebler, P., Pinar, A., and Taymaz, T., 2021, Source characteristics and seismotectonic implications of the 26 September 2019 Mw 5.7 Silivri High-Kumburgaz Basin earthquake and evaluation of its aftershocks at the North Anatolian Fault Zone (Central Marmara Sea, NW Turkey): Geophysical Journal International, v. 227, p. 383–402, https://doi.org/10.1093/gji/ggab233.

Jolivet, R., Jara, J., Dalaison, M., Rouet-Leduc, B., Özdemir, A., Dogan, U., Çakir, Z., Ergintav, S., and Dubernet, P., 2023, Daily to centennial behavior of aseismic slip along the central section of the North Anatolian Fault: Journal of Geophysical Research: Solid Earth, v. 128, https://doi.org/10.1029/2022JB026018.

Karcıoğlu, G., Tank, S.B., Gürer, A., Tolak-Çiftçi, E., Kaya, T., and Tunçer, M.K., 2013, Upper crustal electrical resistivity structures in the vicinity of the Çatalca Fault, Istanbul, Turkey by magnetotelluric data: Studia Geophysica et Geodaetica, v. 57, p. 292–308, https://doi.org/10.1007/s11200-011-0228-6.

Kaya, T., Tank, S.B., Tunçer, M.K., Rokityansky, I.I., Tolak, E., and Savchenko, T., 2009, Asperity along the North Anatolian Fault imaged by magnetotellurics at Düzce, Turkey: Earth, Planets, and Space, v. 61, p. 871–884, https://doi.org/10.1186/BF03353198.

Kaya, T., Kasaya, T., Tank, S.B., Ogawa, Y., Tunçer, M.K., Oshiman, N., Honkura, Y., and Matsushima, M., 2013, Electrical characterization of the North Anatolian Fault Zone underneath the Marmara Sea, Turkey by ocean bottom magnetotellurics: Geophysical Journal International, v. 193, p. 664–677, https://doi.org/10.1093/gji/ggt025.

Lange, D., Kopp, H., Royer, J.Y., Henry, P., Cakir, Z., Petersen, F., and Geli, L., 2019, Interseismic strain build-up on the submarine North Anatolian fault offshore Istanbul: Nature Communications, v. 10, p. 9, https://doi.org/10.1038/s41467-019-11016-z.

Le Pichon, X., İmren, C., Rangin, C., Şengör, A.M.C., and Siyako, M., 2014, The South Marmara Fault: International Journal of Earth Sciences (Geologische Rundschau), v. 103, p. 219–231, https://doi.org/10.1007/s00531-013-0950-0.

Ogawa, Y., and Honkura, Y., 2004, Mid-crustal electrical conductors and their correlations to seismicity and deformation at Itoigawa-Shizuoka Tectonic Line, Central Japan: Earth, Planets, and Space, v. 56, p. 1285–1291, https://doi.org/10.1186/BF03353352.

Özaydın, S., Tank, S.B., and Karaş, M., 2018, Electrical resistivity structure at the North-Central Turkey inferred from three-dimensional magnetotellurics: Earth, Planets, and Space, v. 70, 49, https://doi.org/10.1186/s40623-018-0818-4.

Parsons, T., 2004, Recalculated probability of M $\geq$ 7 earthquakes beneath the Sea of Marmara, Turkey: Journal of Geophysical Research: Solid Earth, v. 109, B05304, https://doi.org/10.1029/2003JB002667.

Schiffer, C., Eken, T., Rondenay, S., and Taymaz, T., 2019, Localized crustal deformation along the central North Anatolian Fault Zone revealed by joint inversion of P-receiver functions and P-wave polarizations: Geophysical Journal International, v. 217, p. 682–702, https://doi.org/10.1093/gji/ggz040.

Schmittbuhl, J., Karabulut, H., Lengliné, O., and Bouchon, M., 2016, Seismicity distribution and locking depth along the Main Marmara Fault, Turkey: Geochemistry, Geophysics, Geosystems, v. 17, p. 954–965, https://doi.org/10.1002/2015GC006120.

Şengör, A.M.C., Tüysüz, O., İmren, C., Sakınç, M., Eyidoğan, H., Görür, N., Le Pichon, X., and Rangin, C., 2005, The North Anatolian Fault: A new look: Annual Review of Earth and Planetary Sciences, v. 33, p. 37–112, https://doi.org/10.1146/annurev.earth.32.101802.120415.

Tank, S.B., Honkura, Y., Ogawa, Y., Matsushima, M., Oshiman, N., Tunçer, M.K., Çelik, C., Tolak, E., and Işıkara, A.M., 2005, Magnetotelluric imaging of the fault rupture area of the 1999 İzmit (Turkey) earthquake: Physics of the Earth and Planetary Interiors, v. 150, p. 213–225, https://doi.org/10.1016/j.pepi.2004.08.033.

Tarancıoğlu, A., Özalaybey, S., and Kocaoğlu, A.H., 2020, Three-dimensional seismic tomographic imaging beneath the Sea of Marmara: Evidence for locked and creeping sections of the Main Marmara Fault: Geophysical Journal International, v. 223, p. 1172–1187, https://doi.org/10.1093/gji/ggaa389.

Turunçtur, B., Eken, T., Chen, Y., Taymaz, T., Houseman, G.A., and Saygin, E., 2023, Crustal velocity images of northwestern Türkiye along the North Anatolian Fault Zone from transdimensional Bayesian ambient seismic noise tomography: Geophysical Journal International, v. 234, p. 636–649, https://doi.org/10.1093/gji/ggad082.

Unsworth, M.J., Malin, P.E., Egbert, G.D., and Booker, J.R., 1997, Internal structure of the San Andreas fault at Parkfield, California: Geology, v. 25, p. 359–362, https://doi.org/10.1130/0091-7613(1997)025<0359:ISOTSA>2.3.CO;2.

Usui, Y., 2015, 3-D inversion of magnetotelluric data using unstructured tetrahedral elements: Applicability to data affected by topography: Geophysical Journal International, v. 202, p. 828–849, https://doi.org/10.1093/gji/ggv186.

Usui, Y., Kasaya, T., Ogawa, Y., and Iwamoto, H., 2018, Marine magnetotelluric inversion with an unstructured tetrahedral mesh: Geophysical Journal International, v. 214, p. 952–974, https://doi.org/10.1093/gji/ggy171.

Wannamaker, P.E., Caldwell, T.G., Jiracek, G.R., Maris, V., Hill, G.J., Ogawa, Y., Bibby, H.M., Bennie, S.L., and Heise, W., 2009, Fluid and deformation regime of an advancing subduction system at Marlborough, New Zealand: Nature, v. 460, p. 733–736, https://doi.org/10.1038/nature08204.

Wessel, P., and Smith, W.H.F., 1995, New version of the generic mapping tools released: Eos (Transactions of the American Geophysical Union), v. 76.

Wollin, C., Bohnhoff, M., Martínez-Garzón, P., Küperkoch, L., and Raub, C., 2018, A unified earthquake catalogue for the Sea of Marmara Region, Turkey, based on automatized phase picking and travel-time inversion: Seismotectonic implications: Tectonophysics, v. 747–748, p. 416–444, https://doi.org/10.1016/j.tecto.2018.05.020.

Yılmaz, Y., Tüysüz, O., Yiğitbaş, E., Genç, S.C., and Şengör, A.M.C., 1997, Geology and tectonic evolution of the Pontides, *in* Robinson, A.G., eds., Regional and Petroleum Geology of the Black Sea and Surrounding Region: AAPG Memoir 68, p. 183–266, https://doi.org/10.1306/M68612C11.

Printed in the USA